Enhanced hydrogen storage in Ni/Ce composite oxides†

Léonard E. A. Berlouis,*[a] Clotilde Jubin,[a] Brian G. McMillan,[a] James Morrow,[a] Mark D. Spicer,[a] Leung P. Tang,[a] Olivier Bordelanne[b] and Michael Weston[b]

Received 3rd July 2007, Accepted 25th September 2007
First published as an Advance Article on the web 10th October 2007
DOI: 10.1039/b710026d

The properties of dried (but not calcined) coprecipitated nickel ceria systems have been investigated in terms of their hydrogen emission characteristics following activation in hydrogen. XRD and BET data obtained on the powders show similarities to calcined ceria but it is likely that the majority of the material produced by the coprecipitation process is largely of an amorphous nature. XPS data indicate very little nickel is present on the outermost surface of the particles. Nevertheless, the thermal analytical techniques (TGA, DSC and TPD-MS) indicate that the hydrogen has access to the catalyst present and the nickel is able to generate hydrogen species capable of interacting with the support. Both unactivated and activated materials show two hydrogen emission features, *viz*. low temperature and high temperature emissions (LTE and HTE, respectively) over the temperature range 50 and 500 °C. A clear effect of hydrogen interaction with the material is that the activated sample not only emits much more hydrogen than the corresponding unactivated one but also at lower temperatures. H_2 dissociation occurs on the reduced catalyst surface and the spillover mechanism transfers this active hydrogen into the ceria, possibly *via* the formation and migration of OH^- species. The amount of hydrogen obtained ($\sim$0.24 wt%) is $\sim$10$\times$ higher than those observed for calcined materials and would suggest that the amorphous phase plays a critical role in this process. The affiliated emissions of CO and CO_2 with that of the HTE hydrogen (and consumption of water) strongly suggests a proportion of the hydrogen emission at this point arises from the water gas shift type reaction. It has not been possible from the present data to delineate between the various hydrogen storage mechanisms reported for ceria.

Introduction

Ceria has been one of the most widely investigated rare earth oxides in the field of catalysis in recent years, particularly in commercial three-way catalysis and fluid catalytic cracking.[1] The high activity of ceria in such reactions is generally attributed to the strength of the Ce^{4+}/Ce^{3+} couple, its oxygen storage capacity and high mobility of oxygen vacancies within the material. The activity and selectivity of the ceria catalyst are greatly enhanced by the presence of noble (Pt, Pd, Rh) as well as base metals (Ni, Cu). The material is versatile, with a host of applications ranging from gas sensors,[2] CO and CH_4 combustion,[3,4] the water gas shift reaction,[5,6] methanol synthesis[7] and as an electrolyte in high temperature fuel cells[8] to name but a few. Composite Ni/Ce systems consisting of metallic Ni as the catalyst on the ceria support are similarly of great interest because of the low cost of Ni and the high catalytic activity of these systems.[9] The Ni/Ce mixed oxides have found applications in the water gas shift (WGS)[5,6,10] in hydrogenation[11] and in oxidation[12] reactions. In the particular area of hydrogen storage, the role of the nickel catalyst impregnated on amorphous activated carbon has been reported.[13,14] It was shown that nickel improves considerably the storage performances of the materials by being involved in a hydrogen spillover mechanism, from catalyst to support. Nickel allows the adsorption of the hydrogen, its dissociation and its migration into the support. It is worth noting that in the studies reported in the literature, the nickel-on-ceria composites were mostly calcined at temperatures in the range of 300–500 °C prior to such catalytic tests. These calcined materials were reduced under hydrogen prior to hydrogenation reactions and their catalytic activity in these reactions correlated well with thermogravimetric measurements and this relationship was considered to be strong evidence for their hydrogen storage ability.[11,15,16]

Thermal analytical studies of calcined ceria based materials have been reported in the literature but the dried, as synthesised material have very rarely been examined using this methodology. Studies of the calcined material have concentrated mostly on the use of thermogravimetric analysis under hydrogen[17] and on thermal programmed reduction[5,16] under reducing atmospheres containing hydrogen to examine the weight changes or amounts of species consumed during the course of the reaction. Differential scanning calorimetry (DSC) performed under hydrogen has been commonly employed to investigate the hydrogen storage ability of hydrides[18] and alloys.[19–21] However, DSC has never been

[a] *WestCHEM, Department of Pure and Applied Chemistry, University of Strathclyde, Glasgow, UK G1 1XL. E-mail: l.berlouis@strath.ac.uk*
[b] *ITI Energy, The Exchange No. 1, 62 Market Street, Aberdeen, UK AB11 5PJ*

† The HTML version of this article has been enhanced with colour images.

directly employed in an in-depth study of the uncalcined composite Ni/Ce oxides, especially in relation to their interaction with hydrogen. Interestingly, in a recent paper, Jalowiecki-Duhamel *et al.*[16] have reported that CeNiAl mixed oxides dried at 100 °C were more active for toluene hydrogenation than the corresponding calcined materials. Indeed, it has been claimed in a recent patent[22] that non-calcined Ni/Ce material has the potential to store higher amounts of hydrogen than has previously been observed in these composite oxides. The aim of this paper was thus to study the hydrogen desorption characteristics of dried (but not calcined) coprecipitated Ni/Ce materials in an inert atmosphere after thermal treatment under pure H_2 (activation) and elucidate the mechanism by which hydrogen is stored and released by this composite material.

Experimental

In this work, the mixed oxides with Ni : Ce = 1 : 10 were prepared by the coprecipitation of hydroxides from mixtures of 3.0×10^{-1} M cerium nitrate ($Ce(NO_3)_3 \cdot 6H_2O$) and 3.0×10^{-2} M nickel ($Ni(NO_3)_2 \cdot 6H_2O$) using either a 1.0 M (KOH) solution or triethylamine (TEA) as the precipitating agent.[23] The reaction was performed at room temperature (or 60 °C for TEA) by adding 150 mL of the salt solution to 400 mL of the base in a well stirred reactor. The precipitate was maintained in the reaction vessel for 3 h under mechanical stirring and was then collected by filtration. For the TEA based synthesis, the product obtained was first washed with 800 mL of ethanol and in all cases, the precipitate was washed with boiling water until the pH of the filtrate was neutral. Over this period, there was a colour change observed in the solid collected, from dark brown to straw yellow, signifying a change in the oxidation state of the cerium. The precipitate was split into 3 batches in order to examine the impact of the drying methods, (*viz.* lyophilisation, or under vacuum at ambient temperature) on the performance of the materials. In the lyophilisation process, the product was suspended in ethanol under sonication and then frozen by the addition of liquid nitrogen. The frozen solid was then dried under vacuum at room temperature and the resulting product was ground to a fine powder by mortar and pestle.

The specific surface areas of the samples were calculated by the BET (Brunauer–Emmett–Teller) method and, for the pore size distribution, the BJH (Barrett, Joyner and Halenda) method was employed. Prior to analysis on the Micromeritics ASAP-2020 porosity analyser, the samples were dried at 60 °C under vacuum and then degassed at 100 °C on the degassing port of analyser. The X-ray powder diffraction apparatus used for all the analyses was the Siemens D500 Diffraktometer, using Cu Kα radiation (λ = 1.5405 Å). The data were acquired using a resolution of 0.05° and an acquisition time of 2 s per step. In the analysis of the Bragg reflection peaks, the full widths at half maximum (FWHM) were corrected for instrumental broadening using a NIST silicon standard (640b). The electron probe micro analyser (EPMA) used for topographical, morphological and chemical analysis of samples was a CAMECA SX100 EPMA system which employed optical microscopy and wavelength dispersive spectroscopy (WDS) system and had three WDS detectors attached. The depth of field for EPMA is *ca.* 5 μm. This technique was particularly useful in building an elemental map of the samples. The XPS instrument used was a Thermo VG sigma probe. A Hiden Isochema Intelligent Gravimetric Analyser (IGA) was used for the thermogravimetric analysis studies. The differential scanning calorimeter employed was the Mettler-Toledo DSC827.

The combined techniques of thermal programmed desorption and mass spectrometry (TPD-MS) were key in evaluating the performance of the samples as this technique allowed emission from the samples to be quantified as the MS was calibrated for H_2 emission using TiH_2 as a desorption standard. The system employed was a Hiden Analytical CATLAB microreactor (TPD) coupled to the HPR20-QIC Atmospheric Gas Analysis System. Typically, helium was used as the inert carrier gas and hydrogen as the reducing/activating agent. The samples were first activated by heating to 250 °C at 10 K min^{-1} under H_2 and then desorbed under He by heating to 800 °C at 10 K min^{-1} with the emission monitored by the MS. Due to differences in instrumental operating conditions, the desorptions were carried out under vacuum in the IGA but under He to 550 °C in the DSC. The DSC and the TPD also operate under a flowing gas mode (40 ml min^{-1}) at atmospheric pressure whereas the IGA operates in static mode.

Results

The measured BET surface areas for most of the synthesised powdered samples, regardless of the drying conditions, were in the range 100–150 m^2 g^{-1}. Pore diameters in the range of 8–12 nm and 12–15 nm were found for the TEA and KOH synthesized samples, respectively. The XRD patterns of the samples are given Fig. 1. It is evident that the fluorite structure of the CeO_2 dominates, with peaks at 2θ = 28.7, 33.2, 47.7 and 56.4° corresponding to the (111), (200), (220) and (311) crystal planes, respectively, of the *Fm3m* structure. Despite the fact that some of the synthesised material contained substantial amounts of Ni (>10 mol%), no reflections were recorded from samples synthesised in TEA which could be associated with the oxides/hydroxides of nickel until the mole ratio of Ni with respect to Ce was above 50 mol%. The calculated lattice parameter (5.42 ± 0.01 Å) from Bragg's law is the same for all

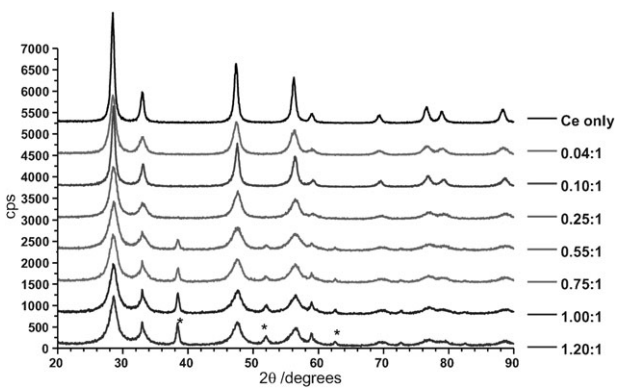

Fig. 1 XRD patterns of various dried, as-synthesized Ni : Ce composite oxides. The main $Ni(OH)_2$ reflections are indicated by the asterisk (*).

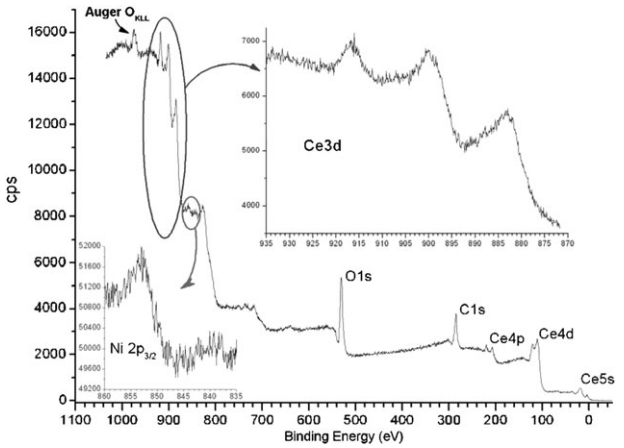

Fig. 2 XPS data for a Ni : Ce 0.1 : 1 composite oxide, showing the high resolution Ni 2p and Ce 3d signals.

of the synthesised samples, regardless of the amount of nickel present in the material. Using the Debye–Scherrer equation, the volume-weighted average crystallite size using data from the three principal reflections was 6.3 ± 0.5 nm in the case of the KOH preparation and 9.2 ± 1.5 nm in the case of the TEA synthesised material. XPS data on the material (Fig. 2) highlighted the presence of Ce, with the 3d features clearly visible at 916 eV, the 4d ones at 120 eV and the 5s one at 20 eV. The signature of the Ce 3d signal is very different from that expected from a fully oxidised ceria, *i.e.* Ce^{4+}.[24] However, the Ni 2p peak expected at 850 eV is only weakly evident, indicating very little Ni on the sample surface. In contrast, the EPMA data (Fig. 3) show a more uniform distribution of Ni and Ce within the composite.

The thermogravimetric analysis data of Fig. 4 shows the results obtained when the samples are activated under hydrogen The initial weight loss at ambient temperature (~2 wt%) under vacuum is due to physisorbed water in the material and subsequent treatment of the sample in a hydrogen atmosphere at 1 bar pressure and 180 °C results in a further weight loss of 1.6 wt%, close to the expected value of 1.82 wt% should the $Ni(OH)_2$ in the composite material be converted to Ni. Note that the corresponding weight loss for NiO going to Ni is

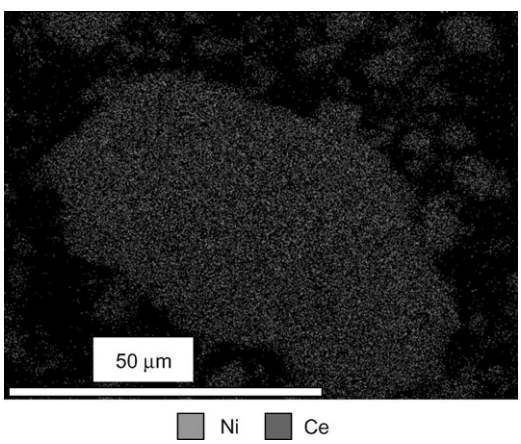

Fig. 3 EPMA data for a Ni : Ce 0.1 : 1 composite oxide, showing the distribution of Ni (green/white) and Ce (red/grey) within the particles.

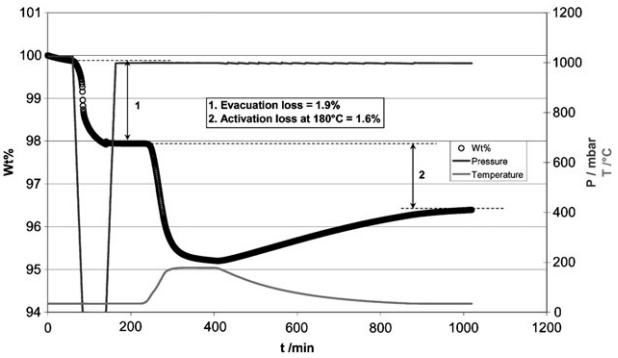

Fig. 4 Thermogravimetric data for a Ni : Ce 0.1 : 1 composite oxide showing weight loss on evacuation and on heating of the sample to 180 °C in 1 bar H_2.

0.87 wt%. On heating the sample in hydrogen up to 400 °C, a total weight loss of 6.0 wt% is observed, with an onset at ~200 °C (Fig. 5). Differential scanning calorimetry (Fig. 6) shows that during the first heating ramp to 250 °C in either H_2 or He, a broad endothermic peak is observed. This is largely due to the conversion of $Ni(OH)_2$ to NiO, ΔH = 51.4 kJ mol^{-1} as the reduction of the NiO to Ni is essentially thermo-neutral (ΔH = 2.5 kJ mol^{-1}) by comparison. For the hydrogen activated material, a broad endothermic feature is observed at ~345 °C during the desorption ramp under He whereas for the He activated sample, the endothermic feature is both sharper and found at the higher temperature of 440 °C. The enthalpies recorded for these events were 25 J g^{-1} and 10 J g^{-1} for the H_2 activated and He activated material, respectively.

The bulk of the testing of the materials for their hydrogen interaction was carried out using the TPD-MS apparatus. Some typical data obtained on this apparatus on heating in He from ambient to 800 °C after He activation are shown in Fig. 7. Two sharp hydrogen emission features, labelled as low temperature and high temperature (LTE and HTE), with peak temperatures of 265 and 406 °C can be observed in these data. Water emission from this sample, corresponding to the conversion of $Ni(OH)_2$ to NiO, is initiated just beyond ~200 °C and this signal then suffers a sudden drop in intensity at 406 °C, coincident with the emission maxima of H_2, CO and CO_2. For the material activated by heating under H_2 between

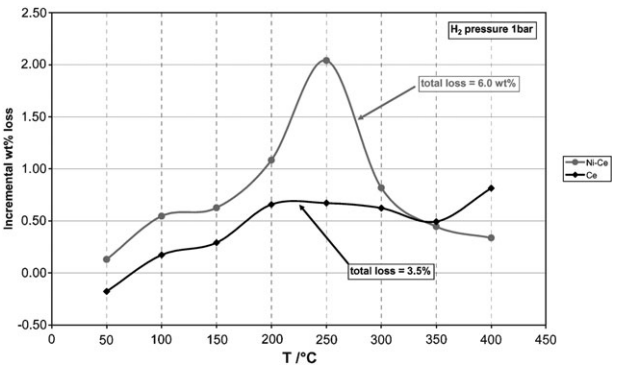

Fig. 5 Incremental weight loss of a Ni : Ce 0.1 : 1 composite oxide on heating from ambient to 400 °C in 1 bar H_2.

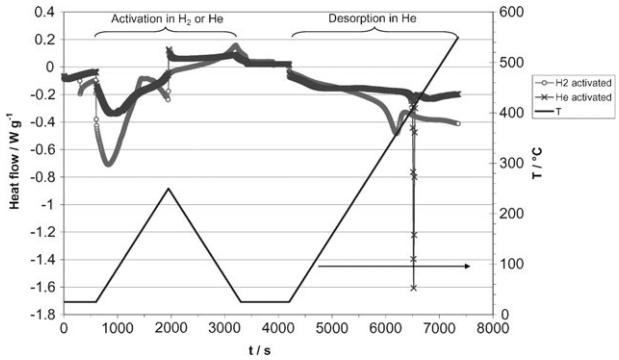

Fig. 6 DSC curves showing the activation and subsequent desorption signals from a Ni : Ce 0.1 : 1 composite oxide. (×) = activation and desorption in He; (○) = activation in 1 bar H_2 and desorption in He.

ambient and 250 °C, two hydrogen emission features are again found in the desorption stage in He but with the peak temperatures lowered to 122 and 374 °C, respectively (Fig. 8). The HTE H_2 emission is again accompanied here with those of CO and CO_2 and a concomitant reduction in the water emission signal. If we compare the total quantity of H_2 emitted in the LTE and HTE events from both experiments, the values obtained are ~0.1 wt% for the He activated sample and 0.24 wt% when the sample has been activated in H_2.

Discussion

Coprecipitation was selected as the method of synthesis in order to improve the interactions between nickel and cerium. The enhancement of the metal-support interactions is commonly supposed to be responsible for a better dispersion of the metal over the support[25,26] which improves the catalytic performances. Some papers have highlighted that the catalytic activity of the metal (*e.g.* Ni or Cu) based on ceria systems prepared by coprecipitation was greater than the ones prepared by impregnation.[26,27] It is also worth noting that the TEA is a weak base and the actual OH^- concentration available at any time will be dependent on its pK_a and this has a value of 10. The $[OH]^-$ availability in the TEA will therefore be considerably lower than for the KOH solution. The precipitation rate in this medium then will be inherently slower

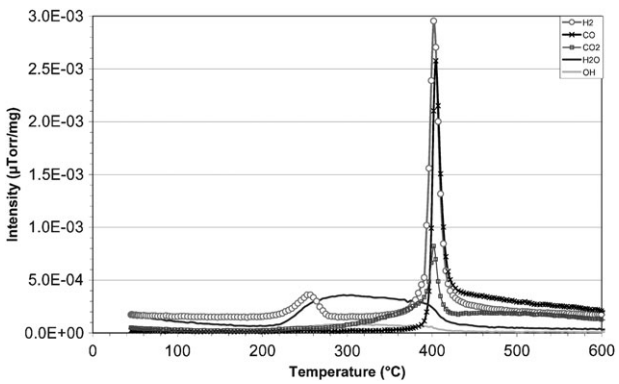

Fig. 7 TPD-MS data for the emission of H_2, CO, CO_2, H_2O and OH as a function of temperature for a Ni : Ce 0.1 : 1 composite oxide following activation in He at 250 °C.

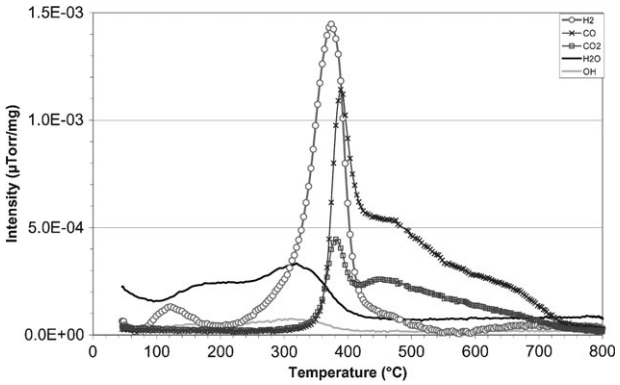

Fig. 8 TPD-MS data for the emission of H_2, CO, CO_2, H_2O and OH as a function of temperature for a Ni : Ce 0.1 : 1 composite oxide following activation in H_2 at 250 °C.

than in either KOH or NaOH at 1.0 M concentration. From the XRD and BET data, it would appear that the as-prepared coprecipitated material displays all the structural characteristics of ceria. The *Fm3m* fluorite structure is the dominant and in some instances, the only crystalline phase identified in the material. This is surprising as the Ni catalyst is present in the precipitated material in a mole ratio of 1 : 10 with Ce but as noted above, no evidence of Ni oxide/hydroxides is apparent in the XRD until mole ratio of Ni with respect to the Ce is at least 50%. Nickel is definitely present in the coprecipitated material since no Ni^{2+} was found from UV-Vis analysis of the reaction solution at the end of the co-precipitation process and inductively coupled plasma-optical emission spectroscopy (ICP-OES) measurements confirmed that the atomic ratio of Ni : Ce in the powdered samples agreed with that used in the synthesis process. It would appear, therefore, that the nickel hydroxide/oxide forms either part of an amorphous phase or crystallites too small to be detected. Indeed, the FWHM of the reflections reveals that even the crystallite phase identified within this mixture consists of very small crystallite domains, in the range from 6 to 11 nm. These measurements would indicate that a substantial part of the synthesised material is of an amorphous nature. Similar data has been reported by Wrobel *et al.*[28] on Ni/Ce samples calcined at 450 °C. They, too, could not detect the presence of the oxides of nickel in their sample below a Ni to Ce atomic ratio of 0.5 and they attributed this to either the nickel oxide being amorphous or the possible formation of a solid solution of Ni into the ceria. The latter is considered unlikely to occur in our samples due to the mild temperatures experienced by the as-synthesised Ni/Ce composite materials. The BET specific surface area values of ~140 $m^2\ g^{-1}$ are consistent with those previously reported,[17,29] albeit for ceria materials with Ni catalyst that have been calcined at temperatures above 300 °C. This is consistent with data of Fig. 9 which indicate that no significant change in the crystallite size of the ceria occurs in air until a temperature of 650 °C is reached. Moreover, the different drying processes, ranging from lyophilisation to vacuum drying at 60 °C, have very little impact on the measured surface area.

Surface analysis using XPS revealed very little Ni on the surface of the particles. Furthermore, as can be seen from the features in the high resolution data shown in Fig. 2, it is clear

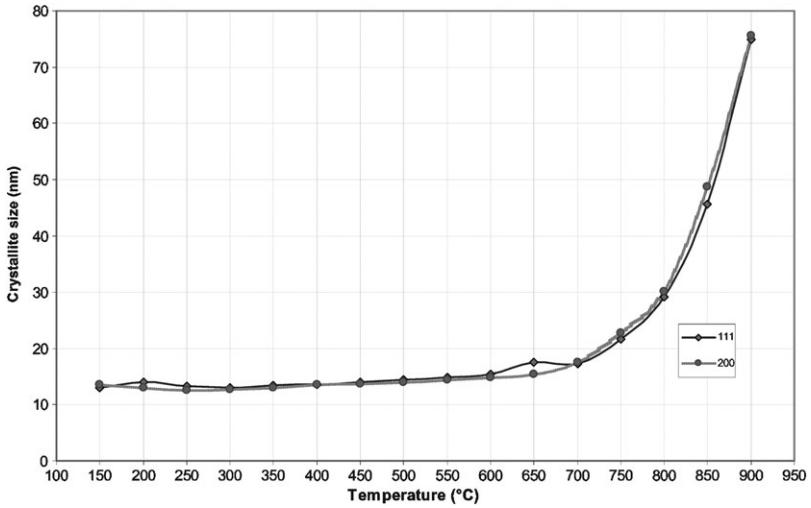

Fig. 9 Crystallite sizes, evaluated from the (111) and (200) reflections, as a function of temperature for a Ni : Ce 0.1 : 1 composite oxide.

that the surface is not solely Ce^{4+} but also contains some Ce^{3+} species.[30] The relatively small amount of surface Ni detected is in direct contrast to both UV-Vis and ICP-OES data which indicated that Ni was present in the material, but the XPS data suggests that this is not at the very top surface. Indeed, the EPMA data confirmed that Ni was uniformly present throughout the particles, at least to within the depth probed ($\sim$5 μm) by this technique. In terms of hydrogen interaction with this composite material, it is important that the Ni oxide/hydroxide has access to the H_2 to enable its reduction and so provide metallic sites on which the hydrogen molecules could dissociate and move within the ceria matrix. Indirect evidence of the reduction process is shown by the IGA data obtained during activation of the Ni/Ce sample in H_2 at 1 bar pressure as the weight loss shows that a substantial proportion of the $Ni(OH)_2$ in the composite material must be undergoing reduction to Ni (Fig. 4). Further evidence of the interaction between hydrogen and the material can be seen from the desorption data in the DSC curves of Fig. 6 which clearly demonstrates that as a result of hydrogen activation, the thermal event associated with the HTE process shifts to lower temperature. The broadness of the endothermic peak suggests that this thermal process comprises a series of events with slightly different activation energies, *viz*. different sites within the material. This is in contrast to the DSC signature from the He activated material which although found at higher temperature is much sharper. This suggests therefore that the process of activation does not lead to a uniform distribution of active nickel cluster sizes and/or sites throughout the composite material or even that different H_2 emission mechanisms are involved. We have noted above that a key component of the hydrogen interaction with this composite material must be the intimate contact between the Ni and the ceria. If this level of interaction is not uniform throughout, then different hydrogen desorption reaction rates may well result. For the He activated material, the hydrogen is emitted by the uncatalysed material at much higher temperature, *i.e*. through the 'normal' decomposition of the composite material and the presence of the nickel, at least initially, does not control this process.

The key data though are those obtained from the TPD-MS measurements (Fig. 8) which shows the clear effects of the interaction of hydrogen with the sample after undergoing activation in hydrogen at 250 °C. Both LTE and HTE hydrogen emission features are shifted to lower temperatures, as observed in the DSC (if only for the HTE event). This is not entirely unexpected since the presence of metallic Ni in the composite material would reduce the activation energies for any hydrogen emission process. Once the reduced catalyst sites are available, the pathway for interaction of the hydrogen with the ceria becomes easier through the spillover process and further reduction of even the ceria itself could result in concomitant creation of oxide vacancies in the ceria lattice as the temperature is increased. Data from the IGA (Fig. 5) however indicate that in 1 bar hydrogen, the reduction of ceria in the composite material is not initiated until a temperature >200 °C is reached. Thus, using our activation conditions, *i.e*. $T < 250$ °C, the amount of reduction of the bulk ceria should be minimal and the hydrogen incorporation into the material must follow a different path.

A comparison of the TDP-MS data for the He activated and hydrogen activated samples (Fig. 7 and 8) indicate that two hydrogen emission peaks are found in both cases, but in the latter, the features occur at a lower temperature. These results are very reproducible, regardless of the age of the sample examined. Two H_2 emission peaks have also been reported by Cuningham *et al*.[31] in their study of H_2 desorption from Rh/CeO_2 samples pre-reduced in H_2 at 100 °C. They suggested that their two observed H_2 emission features (at 220 °C and 470 °C) arose from a competition between the retention of H_2O and/or OH^- species at the micro-interfaces between Rh^0 and ceria facilitating hydrogen spillover to the rare-earth oxide and that of simple adsorption of H on Rh^0. Pre-reduction of their calcined samples at more elevated temperatures led not only to an increase in the amount of hydrogen subsequently re-emitted but also to an increase in the onset temperature for that emission. This was attributed to the increased difficulty in

achieving the reverse spillover in material that lacked the H_2O/OH^- hydrogen transfer bridges. In our samples, the amorphous nature of the material, (which, it must be emphasised, is never calcined) would consist even more so of sites having different activities, *i.e.* interaction between catalyst and bulk, and the two emissions observed would simply be reflecting this. The higher temperature observed for the hydrogen emissions from the He activated sample in relation to the hydrogen activated one then could be linked to the lack of availability of metallic catalyst sites during the 'decomposition' of the material.

The other striking features of the TPD-MS data shown in Fig. 7 and 8 are that for the HTE process in both He activated and hydrogen activated materials, the emission of hydrogen occurs together with CO and CO_2 but with a consumption of water. This hydrogen emission could involve a water gas shift (WGS) type reaction but this would necessitate the release of CO by the material at this temperature, *i.e.* from the thermal decomposition of carbonate species in the sample. An inspection of the H_2O and H_2 curves in the data of Fig. 7 and 8 in the HTE region shows that the amount of water consumed at 350 and 400 °C, respectively, is far smaller than the amount of H_2 emitted. The WGS reaction therefore cannot solely account for all the hydrogen emitted and another mechanism yielding hydrogen at this temperature must be present. The source of CO (and indeed CO_2) in the material could be from carbonates introduced during the synthesis, either directly from the raw materials, the alkaline (KOH or TEA) solutions employed or through absorption of CO_2 from the air during the filtration and the washing stages. Indeed, it would be difficult to totally eliminate carbonate from the process unless the alkaline solution was prepared in a CO_2 free environment. Nevertheless, synthesis in such an environment and the characterisation of the samples so produced is currently under way in our laboratory.

A survey of the literature pertinent to the interaction of H_2 with ceria has revealed several potential mechanisms for storage of hydrogen species by these materials. The majority of the work has dealt directly with the interaction of H_2 with ceria which has been prepared by a variety of routes but then always calcined. As has been discussed, these materials are different from our own materials which have not been subjected to any temperature treatment above 250 °C prior to analysing the hydrogen emission from the samples. A common theme in all the reported work is that CeO_2 based materials, when heated under H_2-containing atmospheres can take up a small amount of hydrogen and undergo (reversible) reduction at temperatures above *ca.* 327 °C.[32] At somewhat higher temperatures irreversible reduction to the sesquioxide (Ce_2O_3) is dominant. There is some disagreement, however as to the nature of this hydrogen uptake. Bernal *et al.*[33] has suggested that the process can entirely be accounted for as a surface phenomenon, with the quantity of hydrogen estimated at ~0.017 wt%. Fierro *et al.*[34] on the other hand suggested, on the basis of no observed increase in the intensity of OH bands in the IR spectrum, that the process was primarily a bulk phenomenon and they found their hydrogen level to be ~0.07 wt%. Perrichon *et al.*[35] and Bruce *et al.*,[36] on the other hand, believed the process to be a mixture of bulk and surface events, on the grounds that H_2 uptake appears to have a constant part (bulk) and a part which varied with surface area. It was suggested that the bulk process led to a "bronze" type material H_yCeO_{2-x}, while the surface interaction led to a formation of hydroxyl ions and/or water. Sohlberg *et al.*[37] undertook calculations which showed it to be possible for an H species to reside within the O_8 cube in the CeO_2 lattice. An H atom placed in this space migrates to associate with a single O^{2-} ion, forming hydroxide. This process was evaluated and shown to be spontaneous below *ca.* 650 °C. On the other hand, placing a hydride ion in an octahedral hole bounded by 6 Ce ions resulted in relaxed structures unstable with respect to dissociation into CeO_2 and H_2. In his review of interaction of H_2 with oxides, Norby *et al.*[38] pointed out that in the majority of cases the expected form of hydrogen within a lattice was as H^+ since the electron potential within an oxide is such that the hydrogen is expected to be fully ionised. The process could most simply be described by

$$H_2 + 2O_O^* \rightarrow 2OH_O^\bullet + 2e^-$$

where the O subscript relates to the oxygen site in the ceria lattice. A similar outcome was also possible by the interaction of water with a surface vacancy,[38] *viz.*

$$H_2O + V_O^{\bullet\bullet} \rightarrow O_O^* \rightarrow 2OH_O^\bullet$$

The possibility of a hydride ion residing in an oxide lattice was considered in their study to be unreasonable, despite a number of reports having appeared in the literature[39] claiming just such a species (*e.g.* $LaSrCoO_3H_{0.7}$—described as a Perovskite-related material with hydride ions occupying oxygen sites).

For our composite material, it is likely that a prerequisite for hydrogen incorporation into the composite material is the reduction of the nickel oxide catalyst during activation, in order to allow the subsequent dissociation of the H_2 on the catalyst surface and so provide the hydrogen species to permeate/diffuse into the storage matrix. Ramaroson *et al.*[40] have suggested that an electron enrichment of the Ni catalyst can result from the reduction of the surface oxide in the ceria through the spillover mechanism,

$$Ni^0 - H + O_S^{2-} \rightarrow OH_S^- + Ni^0 + e^-$$

with the liberated electron migrating from the valence band of the ceria to the ceria–nickel interface. According to Wrobel *et al.*,[11] in the anionic-defected solid solution formed in the Ce–Ni–O system, the interaction of the hydrogen with the Ni catalyst leads not only to the homolytic dissociation of the hydrogen molecule and to the formation of an oxygen vacancy *via*

$$2Ce^{4+} + O^{2-} + 2H \rightarrow 2Ce^{3+} + H_2O + V_O^{\bullet\bullet}$$

but furthermore, through the reaction

$$2Ce^{4+} + Ni^0 \rightarrow 2Ce^{3+} + Ni^{2+}$$

a strong interaction, *viz.*, an electronic exchange is established between the two metal cations which enhances the hydrogen spillover effect as well as preventing the sintering of the nickel atoms. To allow this process to occur effectively, an intimate contact between the metal catalyst and the bulk ceria is

essential. The thermal analysis data show that in our material, the coupling between catalyst and bulk does exist and the presence of the catalyst affects the hydrogen emission profiles, as observed in the TPD-MS and related DSC measurements. However, there is no evidence from our data that lattice site substitution by the Ni into the ceria lattice occurs, *i.e.* the formation of a solid solution of Ni–Ce–O. Thus in our system, a likely route for hydrogen incorporation could first be the dissociation of the hydrogen on the reduced Ni surface and subsequently, due to the strong coupling between catalyst and bulk, hydrogen spillover to the latter could occur resulting in the formation of OH^-. Hydrogen storage within the matrix could thus be as 'OH'. The presence of OH^- could also explain why in our uncalcined material, a strong hydrogen emission, albeit at more elevated temperatures than found after H_2 activation, is also found without prior exposure of the sample to H_2. One also has to bear in mind that the material is substantially amorphous. Indeed, the movement of this hydrogen species through this amorphous phase would be considerably easier than through large crystallites and so would enable rapid access of the hydrogen to the small crystallites in this composite material. It is clear that the amount of H_2 released by our samples is some 10× higher (0.24 wt% *cf.* 0.01 wt%) than that previously reported on calcined Ni/Ce composite material and the amorphous nature of the as-synthesised material must play a role in this.

Conclusions

The properties of dried (but not calcined) coprecipitated nickel ceria systems have been investigated in terms of their hydrogen emission characteristics before and after activation in hydrogen. The physical structure as seen by XRD and BET measurements shows similarities to calcined ceria but there is strong evidence to suggest that the majority of the material is in an amorphous state rather than crystalline. Although XPS data indicate very little nickel on the outermost surface of the particles, the thermal analytical techniques (TGA, DSC and TPD-MS) indicate that the hydrogen has access to the nickel catalyst present in the composite material. Thus, the nickel is able to produce hydrogen species capable of interacting with the support. Although both He activated and H_2 activated materials show emission of hydrogen, the emissions from the H_2 activated sample is greater and occurs at lower temperatures. The affiliated emissions of CO and CO_2 with that of the HTE hydrogen (and consumption of water) strongly suggest a proportion of the hydrogen emission at this point arises from the water gas shift type reaction. It has not been possible from the present data to delineate between the various hydrogen storage mechanisms reported for ceria. H_2 dissociation occurs on the nickel surface and the spillover mechanism transfers this active hydrogen into the ceria, possibly *via* the formation and migration of OH^- species. The amount of hydrogen obtained (~0.24 wt%) is ~10× higher than those observed for calcined materials and would suggest that the amorphous phase plays a critical role in this process.

Acknowledgements

The authors gratefully acknowledge the technical and financial support received from ITI Energy (Scotland) for this project.

References

1 A. Trovarelli, C. de Leitenburg, M. Boaro and G. Dolcetti, *Catal. Today*, 1999, **50**, 353.
2 U. Lampe, J. Gerblinger and H. Meixner, *Sens. Actuators, B*, 1992, **7**, 787.
3 L.-S. Kau, D. J. Spira-Salomon, J. E. Penner-Hahn, K. O. Hodgson and E. I. Solomon, *J. Am. Chem. Soc.*, 1989, **109**, 6433.
4 A. Martínez-Arias, A. B. Hungría, M. Fernández-García, J. C. Conesa and G. Munuera, *J. Phys. Chem. B*, 2004, **108**, 17983.
5 Y. Li, Q. Fu and M. Flytzani-Stephanopoulos, *Appl. Catal., B*, 2000, **27**, 179.
6 G. Jacobs, E. Chenu, P. M. Patterson, L. Williams, D. Sparks, G. Thomas and B. H. Davis, *Appl. Catal., A*, 2004, **258**, 203.
7 E. A. Shaw, T. Rayment, A. P. Walker, R. M. Lambert, T. Gauntlett, R. J. Oldman and A. Dent, *Catal. Today*, 1991, **9**, 197.
8 S. Park, J. M. Vohs and R. J. Gorte, *Nature*, 2000, **404**, 265.
9 D. K. Kim, K. Stöwe, F. Müller and W. F. Maier, *J. Catal.*, 2007, **247**, 101.
10 S. Hilaire, X. Wang, T. Luo, R. J. Gorte and J. Wagner, *Appl. Catal., A*, 2001, **215**, 271.
11 G. Wrobel, C. Lamonier, A. Bennani, A. D'Huysser and A. Aboukaïs, *J. Chem. Soc., Faraday Trans.*, 1996, **92**, 2001.
12 T. Zhu and M. Flytzani-Stephanopoulos, *Appl. Catal., A*, 2001, **208**, 403.
13 M. Zieliński, R. Wojcieszak, S. Monteverdi, M. Mercy and M. M. Bettahar, *Catal. Commun.*, 2005, **6**, 777.
14 M. Zieliński, R. Wojcieszak, S. Monteverdi, M. Mercy and M. M. Bettahar, *Int. J. Hydrogen Energy*, 2007, **32**, 1024.
15 L. Jalowiecki-Duhamel, J. Carpentier, E. Payen and F. Heurtaux, *Int. J. Hydrogen Energy*, 2007, **32**, 2593.
16 L. Jalowiecki-Duhamel, J. Carpentier and A. Ponchel, *Int. J. Hydrogen Energy*, 2007, **32**, 2439.
17 C. Lamonier, A. Ponchel, A. D'Huysser and L. Jalowiecki-Duhamel, *Catal. Today*, 1999, **50**, 247.
18 A. Borgschulte, U. Bösenberg, G. Barkhodarian, M. Dornheim and R. Bormann, *Catal. Today*, 2007, **120**, 262.
19 M. Kondo, K. Asano and Y. Iijima, *J. Alloys Compd.*, 2005, **393**, 269.
20 G. Srinivas, V. Sankaranarayanan and S. Ramprabhu, *Int. J. Hydrogen Energy*, 2007, **32**, 2480.
21 L. E. A. Berlouis, N. Comisso and G. Mengoli, *J. Electroanal. Chem.*, 2005, **586**, 105.
22 D. Huguenin and O. Bordelanne, Patent WO 2006/003475, 2006.
23 L. Jalowiecki-Duhamel, A. Ponchel and C. Lamonier, *Int. J. of Hydrogen Energy*, 1999, **24**, 1083.
24 D. R. Mullins, S. H. Overbury and D. R. Huntley, *Surf. Sci.*, 1998, **409**, 307.
25 A. M. Fuente, G. Pulgar, F. González, C. Pesquara and C. Blanco, *Appl. Catal., A*, 2001, **208**, 35.
26 K. V. R. Chary, P. V. R. Rao and V. Vishwanathan, *Catal. Commun.*, 2006, **7**, 974.
27 C. Zerva and C. J. Philippopoulos, *Appl. Catal., B*, 2006, **67**, 105.
28 G. Wrobel, M. P. Sohier, A. D'Huysser and J. P. Bonnelle, *Appl. Catal., A*, 1993, **101**, 73.
29 C. Lamonier-Dulongpont, PhD Thesis, Université des Sciences et Technologies de Lille, France, 1994.
30 J. E. Spanier, R. D. Robinson, F. Zhang, S.-W. Chan and I. P. Herman, *Phys. Rev. B*, 2001, **64**, 245407.
31 J. Cunningham, D. Cullinane, J. Sanz, J. M. Rojo, X. A. Soria and L. G. Fierro, *J. Chem. Soc., Faraday Trans.*, 1992, **88**, 3233.
32 M. Boaro, M. Vicario, C. de Leitenburg, G. Dolcetti and A. Trovarelli, *Catal. Today*, 2003, **77**, 407.
33 S. Bernal, J. Calvino, G. A. Cifredo, J. M. Gatica, J. A. Pérez Omil and J. M. Pintado, *J. Chem. Soc., Fraday Trans.*, 1993, **89**, 3499.
34 J. L. G. Fierro, J. Soria, J. Sanz and J. M. Rojo, *J. Solid State Chem.*, 1987, **66**, 154.

35 A. Laachir, V. Perrichon, A. Badri, J. Lamotte, E. Catherine, J. C. Lavalley, J. El Fallah, L. Hilaire, F. Le Normand, E. Quéméré, G. N. Sauvion and O. Touret, *J. Chem. Soc., Faraday Trans.*, 1991, **87**, 1601.
36 L. A. Bruce, M. Hoang, A. E. Hughes and T. W. Turney, *Appl. Catal., A*, 1996, **134**, 351.
37 K. Sohlberg, S. T. Pantelides and S. J. Pennycook, *J. Am. Chem. Soc.*, 2001, **123**, 6609.
38 M. Widerøe, N. Kochetova and T. Norby, *J. Chem. Soc., Dalton Trans.*, 2004, **147**, 3147.
39 M. Hayward, E. J. Cussen, J. B. Claridge, M. Bieringer, M. J. Rosseinsky, C. J. Kiely, S. J. Blundell, I. M. Marshall and F. L. Pratt, *Science*, 2002, **295**, 1882.
40 E. Ramaroson, J. F. Tampere, M. F. Guilleux, F. Vergrand, H. Roulet and G. Dufour, *J. Chem. Soc., Faraday Trans.*, 1992, **88**, 1211.